Case Studies in Mechanical Systems and Signal Processing 4 (2016) 19–27

Contents lists available at ScienceDirect

Case Studies in Mechanical Systems and Signal Processing

journal homepage: www.elsevier.com/locate/csmssp

An effective trajectory planning method for simultaneously suppressing residual vibration and energy consumption of flexible structures

Akira Abe

Department of Systems, Control and Information Engineering, National Institute of Technology, Asahikawa College, 2-2-1-6 Shunkodai, Asahikawa, Hokkaido 071-8142, Japan

ARTICLE INFO

Article history:
Received 20 May 2016
Received in revised form 25 July 2016
Accepted 19 August 2016
Available online 27 August 2016

Keywords:
Energy saving
Vibration control
Trajectory planning
Flexible structure
Polynomial function
Metaheuristics

ABSTRACT

This paper presents a proposal for a minimum energy feedforward control technique for flexible structures to suppress residual vibrations in point-to-point (PTP) motion. In the proposed method, the trajectory profile of the PTP motion is generated through a cycloidal function whose input is the output of a polynomial function. The obtained trajectory is dependent upon the coefficients of the polynomial function. To achieve the suppression of the residual vibration as well as the operating energy of this PTP motion, the coefficients are tuned by metaheuristic algorithms. In the numerical simulations, we investigated the PTP motions of a single-link flexible manipulator and a robotic arm attached to a flexible link. The simulation results were compared with those of previous studies, revealing the effectiveness of the proposed method.

1. Introduction

Flexible manipulators, which comprise thin slender arms, can enable higher-speed operation and lower energy consumption because their weight is typically lower than that of a rigid manipulator. Moreover, light-weight manipulators are beneficial for cutting down transport costs of industrial or space robots. Therefore, flexible manipulators are superior to rigid manipulators in the above respects. However, it is well known that flexible manipulators are easily deformed due to their low flexibility; therefore, unwanted vibrations, which have a harmful effect on working effectiveness, occur easily. Thus, to avoid the unwanted vibrations of flexible manipulators, many researchers have attacked the vibration problem and have presented various control schemes [1–3]. In particular, trajectory planning methods are one of the best ways to control the vibrations for point-to-point (PTP) motion tasks of flexible manipulators [4–19]. However, to the best of the author's knowledge, studies on reducing the operation energy required to run manipulators have been limited to rigid manipulators (e.g., [20–22]). A trajectory planning method that simultaneously suppresses the residual vibration and driving energy of a flexible manipulator has not been presented. Energy savings for flexible manipulators are very important for space robots because there is a limited amount of energy available for tasks.

With this background in mind, a trajectory planning method was developed; it enables to simultaneously minimize residual vibrations and the driving energy for a single-link flexible manipulator [23] and a robotic arm mounted on a flexible link [24]. For this trajectory planning method, an artificial neural network (ANN) was employed to generate the joint angles

E-mail address: abe@asahikawa-nct.ac.jp (A. Abe).

http://dx.doi.org/10.1016/j.csmssp.2016.08.001

of both manipulator [23] and robotic arm [24]. Because the generated joint angle trajectory depends on the parameters of the ANN, we tuned the parameters to simultaneously minimize the residual vibration and driving energy. Therefore, for this minimization, metaheuristic algorithms were utilized. One notable feature of the trajectory planning method is that one can easily construct an energy-conserving open-loop controller because the methodology is based on metaheuristic algorithms. However, although the ANN can generate a smooth trajectory, many parameters are required; thus, the computational cost to do so is relatively high. Conversely, the author in reference [25] also dealt with PTP motion of two flexible links attached to one motor hub and proposed trajectory planning methodology to cancel the residual vibrations; for this, a combination of cycloidal and polynomial functions was utilized to generate the trajectory. It was demonstrated that by tuning only four parameters multimode vibration control could be achieved. Because this trajectory planning method enables the easy generation of a smooth motion, there is a strong likelihood that further energy saving of flexible structures will be achieved by using it.

In this study, we investigate the possibility of further reducing the driving energy for PTP motion of flexible structures; to achieve this, we employ a combination of cycloidal and polynomial functions to generate the trajectory [25]. The trajectory profile developed here is dependent upon the coefficients of the polynomial function. To accomplish the minimization of not only the driving energy but also the residual vibration of the PTP motion, the coefficients were tuned by metaheuristic algorithms; thus, the optimal trajectory can be obtained. We performed the numerical simulations for a single-link flexible manipulator and a robotic arm attached to a flexible link. Then, we compared the results with those of previous studies [23,24]. This comparison demonstrates that the proposed method is superior at increasing energy savings. The main contribution of this paper is to show that the trajectory planning method developed here for a PTP motion of a flexible manipulator system can achieve further energy saving with zero residual vibrations.

2. Optimal trajectory profile

In the present study, we studied a PTP motion task of a flexible manipulator system that has one revolution joint; we try to generate an optimal trajectory enabling the suppression of residual vibration under minimum energy conditions. The optimal trajectory profile of the joint angle is given as follows using a cycloidal function:

$$\theta_{opt}(t) = (\theta_E - \theta_S)\left\{U(t) - \frac{1}{2\pi}\sin[2\pi U(t)]\right\} + \theta_S, \tag{1}$$

where θ_S, θ_E, and T_E are the initial angle, target angle, and travelling time for the PTP motion, respectively. The input function of time t is denoted by $U(t)$. The differentiation of Eq. (1) yields the profiles of the angular velocity and acceleration:

$$\dot{\theta}_{opt}(t) = 2(\theta_E - \theta_S)\sin^2[\pi U(t)]\,\dot{U}(t), \tag{2}$$

$$\theta_{opt}(t) = (\theta_E - \theta_S)\sin[\pi U(t)]\,\{2\pi\cos[\pi U(t)]\,\dot{U}^2(t) + \sin[\pi U(t)]\,U(t)\}. \tag{3}$$

For the cycloidal motion, the input function is defined as

$$U(t) = \frac{t}{T_E}. \tag{4}$$

We can confirm from Eqs. (1)–(4) that the cycloidal motion naturally satisfies the boundary conditions as

$$\left.\begin{array}{l} \theta_{opt} = \theta_S, \dot{\theta}_{opt} = \theta_{opt} = 0, \text{for} U = 0 (t = 0) \\ \theta_{opt} = \theta_E, \dot{\theta}_{opt} = \theta_{opt} = 0, \text{for} U = 1 (t = T_E) \end{array}\right\}; \tag{5}$$

that is, smooth motion is generated, in which the velocity and acceleration are equal to zero at the start and end points of the PTP motion. However, the cycloidal motion induces large residual vibrations in the PTP motion [13,16,23–25].

Thus, in the present study, we attempt to express the input function as

$$U(t) = \frac{t}{T_E} + (1 - T^2)\sum_{n=1}^{N} a_n T^{n-1}, \tag{6}$$

where

$$T = -1 + \frac{2t}{T_E}. \tag{7}$$

The input function in Eq. (6) meets the conditions $U = 0$ for $t = 0$ and $U = 1$ for $t = T_E$; that is to say, smooth motion satisfying the boundary conditions in Eq. (5) can be generated. The polynomial function in Eq. (6) shapes the input of the cycloidal function and then an arbitrary trajectory profile can be obtained from Eq. (1) [25]. In this case, the trajectory profile is dependent upon the coefficients a_n in the polynomial function. Hence, it is necessary to tune the coefficients so as to simultaneously minimize the residual vibration and operating energy of a flexible manipulator system. In the present study, we employ a metaheuristic algorithm as the tuning method because metaheuristics have the advantage that the calculation of derivatives in the optimization process is not needed. Finally, this tuning can yield the optimal trajectory, details of which will be presented in the next section.

3. Case study

To evaluate the effectiveness of the optimal trajectory profile based on the cycloidal and polynomial functions, we performed numerical simulations for a single-link flexible manipulator and a robot manipulator mounted on a flexible link. Some results of these simulations are presented in this section.

3.1. Single-link flexible manipulator

The mathematical model of the single-link flexible manipulator with tip mass that considered in this subsection is shown in Fig. 1. The flexible manipulator is clamped to a rigid hub whose radius is a. Here, θ is the joint angle while w and u are the transverse and axial displacements of the flexible manipulator, respectively. It should be noted that u represents the axial shortening caused by the large bending deformation and s is the coordinate along the deformed configuration of the flexible manipulator [13]. In the experimental setup [23], a brass plate of length 475 mm, width 50 mm, and thickness 1 mm was used as the flexible manipulator whose tip mass weighed 36 g. The equations of motion for the flexible manipulator are given as follows:

$$\alpha_1\theta + \alpha_2 W + c\dot{\theta} = \tau, \tag{8}$$

$$W + 2\zeta\omega\dot{W} + \omega^2 W + \beta_1\theta + \beta_2\dot{\theta}^2 W = 0, \tag{9}$$

where W and τ are the amplitude of the first vibrational mode and the torque applied at the joint, respectively. The values of the coefficients in Eqs. (8) and (9) are as follows [23]:

$$\left.\begin{array}{l}\alpha_1 = 2.383 \times 10^{-2}\,[\mathrm{kgm}^2]\,, \alpha_2 = 9.261 \times 10^{-2}[\mathrm{kgm}]\,, c = 3.091 \times 10^{-2}[\mathrm{Nms}], \beta_1 = 2.555 \times 10^{-1}[\mathrm{m}] \\ \beta_2 = 2.614 \times 10^{-1}[-], \zeta = 9.636 \times 10^{-3}[-], \omega = 10.43[\mathrm{rad/s}]\end{array}\right\}. \tag{10}$$

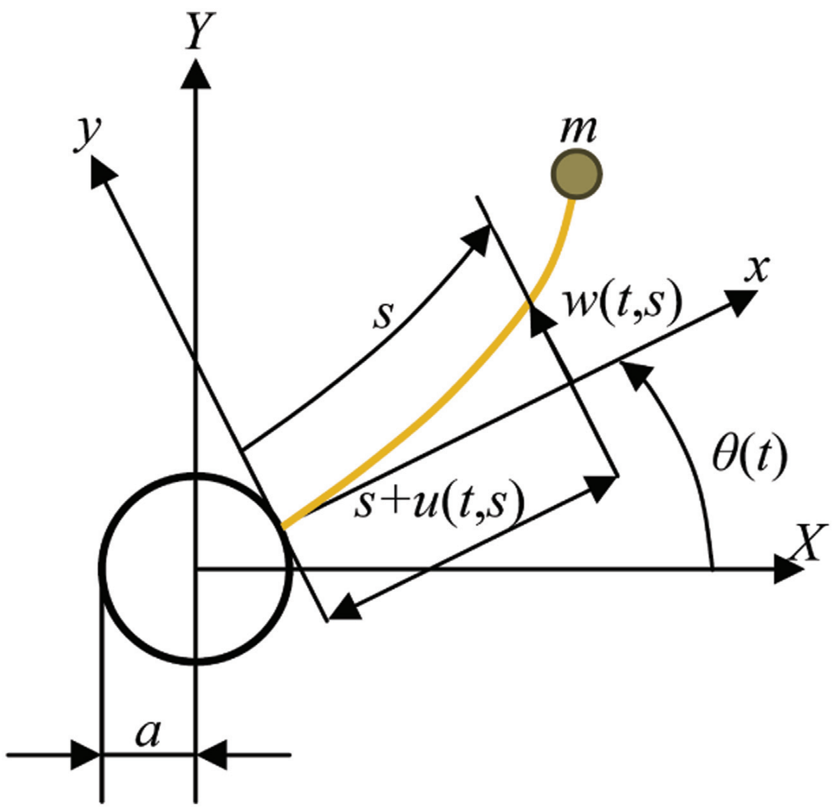

Fig. 1. Schematic of a single-link flexible manipulator.

PTP motion of a flexible manipulator for a fixed travelling time T_E and target angle θ_E is considered here. We attempted to generate the optimal trajectory for simultaneously suppressing the residual vibration and driving energy by using the approach developed in the previous section. In this case, we set $\theta_S = 0$ because the dynamics of the flexible manipulator are not dependent on the initial angle. For this purpose, we defined the objective functions as follows:

$$F_1 = \max_{t \in S}[|w(t,l)|],\ (S : T_E \le t \le T_E + 1\,\text{s}),\ F_2 = \int_0^{\theta_E} |\tau|\, d\theta. \tag{11}$$

Here, F_1 and F_2 denote the maximum tip displacement within 1 s after the positioning and the operating energy until the positioning, respectively. By tuning the coefficients a_n in Eq. (6) to simultaneously minimize the two objective functions in Eq. (11), the optimal trajectory is obtainable. The algorithm of the optimal trajectory generation is summarized below.

First of all, we set a driving condition (i.e., target angle θ_E and travelling time T_E), while the coefficients a_n are the optimized parameters. By using the input function in Eq. (6), the trajectory profile is calculated from Eqs. (1)–(3). Next, numerical integration of Eq. (9) using the calculated trajectory profile yields the displacement of the flexible manipulator (i.e., the objective function F_1 is obtained). The driving torque is obtained from inverse dynamics analysis of Eq. (8), and then the objective function F_2 is calculated. To simultaneously minimize the two objective functions, the coefficients a_n are tuned by vector evaluated particle swarm optimization (VEPSO) [26], which is a multi-objective optimization method. Finally, this optimization approach serves to generate the optimal trajectory. It should be noted that the residual vibration suppression and energy conservation of the flexible manipulator can be attained by driving the joint angle along the obtained optimal trajectory, that is, the proposed method is categorized as an open-loop control considering that the sensors measuring the vibrations are not required.

In the VEPSO algorithm for generating the optimal trajectory, the number of particles in each swarm and the maximum number of iterations are set, respectively, to 100 and 200, which are same as in a previous study [23]. The search space of the optimized parameters is as follows:

$$a_n \in [-0.2, 0.2], \quad (n = 1, 2, \cdots, N). \tag{12}$$

The optimal trajectory profile also depends on the number of terms N of the polynomial function in Eq. (6). First of all, we investigate the effects of the number of terms on the residual vibration suppression and operating energy. Fig. 2 shows the simulation results obtained from the proposed method under the driving condition ($\theta_E = \pi/6$ rad, $T_E = 0.8$ s), in which the green, red, and blue lines denote the results for $N = 2$, 4, and 6, respectively. Additionally, the black line indicates the results obtained from the cycloidal motion (i.e., Eq. (4) is employed as the input function). The joint angle, angular velocity, tip displacement of the flexible manipulator, and motor torque are illustrated in Fig. 2(a), (b), (c), and (d), respectively. The values of the coefficients a_n obtained for the optimal solution are listed in Table 1. As portrayed in Fig. 2(c), a large residual vibration with an amplitude of about 7.7 cm after positioning (after $t = 0.8$ s) occurs when the joint angle is rotated along the cycloidal motion. Moreover, motor torque that keeps the joint angle at the target angle against the residual vibration is

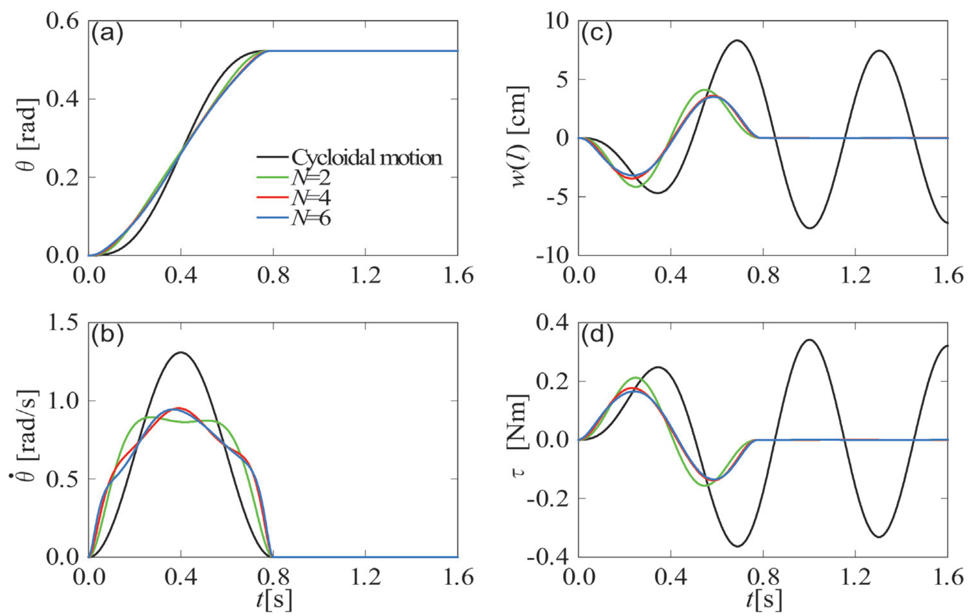

Fig. 2. Effect of the number of terms of the polynomial function on the optimal trajectory ($\theta_E = \pi/6$ rad, $T_E = 0.8$ s): (a) joint angle, (b) angular velocity, (c) tip displacement, and (d) motor torque.

Table 1
Optimized parameters under the driving condition ($\theta_E = \pi/6$ rad, $T_E = 0.8$ s).

N	a_1	a_2	a_3	a_4	a_5	a_6
2	3.347×10^{-3}	-1.697×10^{-1}	–	–	–	–
4	-1.690×10^{-3}	-1.367×10^{-1}	-1.951×10^{-2}	-1.971×10^{-1}	–	–
6	-1.889×10^{-3}	-1.427×10^{-1}	-4.247×10^{-2}	-1.187×10^{-1}	4.800×10^{-2}	-1.890×10^{-1}

Table 2
Effect of the number of terms N on the operating energy F_2 [J] under the driving condition ($\theta_E = \pi/6$ rad, $T_E = 0.8$ s).

$N = 2$	$N = 4$	$N = 6$
6.29×10^{-2}	5.26×10^{-2}	5.15×10^{-2}

induced in cycloidal motion. Conversely, the present method generates smooth trajectory profiles thereby cancelling the residual vibration perfectly. It should be noted that the optimal trajectory calculated for only $N = 2$ accomplishes residual vibration suppression (i.e., vibration control is achieved by tuning only two coefficients of a_n in Eq. (6)). Incidentally, it is also interesting that with an increase in the number of terms, the maximum tip displacement during the PTP motion reduces. Therefore, we can say that the proposed method is effective for vibration control. The operating energy, which is defined in Eq. (11), is listed in Table 2. It can be seen in Table 2 that increasing the number of terms also decreases the operating energy. Consequently, it is revealed that although $N = 2$ number of terms is sufficient to cancel the residual vibration, increasing the number of terms is necessary for energy saving. In the numerical simulations presented below, the number of terms was set to $N = 6$ because the operating energy was not further decreased for numbers greater than 6.

To check the validity of our optimal trajectory generation method for the flexible manipulator, we compared our results with those of a previous study [23] in which an ANN was employed to generate an optimal trajectory. The time histories of the joint angle, angular velocity, tip displacements, and motor torque under the driving condition ($\theta_E = \pi/6$ rad, $T_E = 0.8$ s) are illustrated in Fig. 3, in which the results obtained from our method and from the previous study are depicted in blue and orange lines, respectively. As shown in Fig. 3(c), there is no significant difference in residual vibration suppression between both approaches, whereas in the proposed method the maximum tip displacement until positioning is small compared with that in the previous study. Table 3 lists a comparison of the operating energies obtained by the present and previous methods for three driving conditions: ($\theta_E = \pi/6$ rad, $T_E = 0.8$ s), ($\theta_E = \pi/2$ rad, $T_E = 1.0$ s), and ($\theta_E = \pi/2$ rad, $T_E = 1.1$ s). It is worth noting that for all driving conditions the values obtained by the present method were smaller than those obtained using the previous method based on an ANN. Therefore, we can confirm that the present method is valid and effective not only for vibration control but also for energy saving in a flexible manipulator with PTP motion.

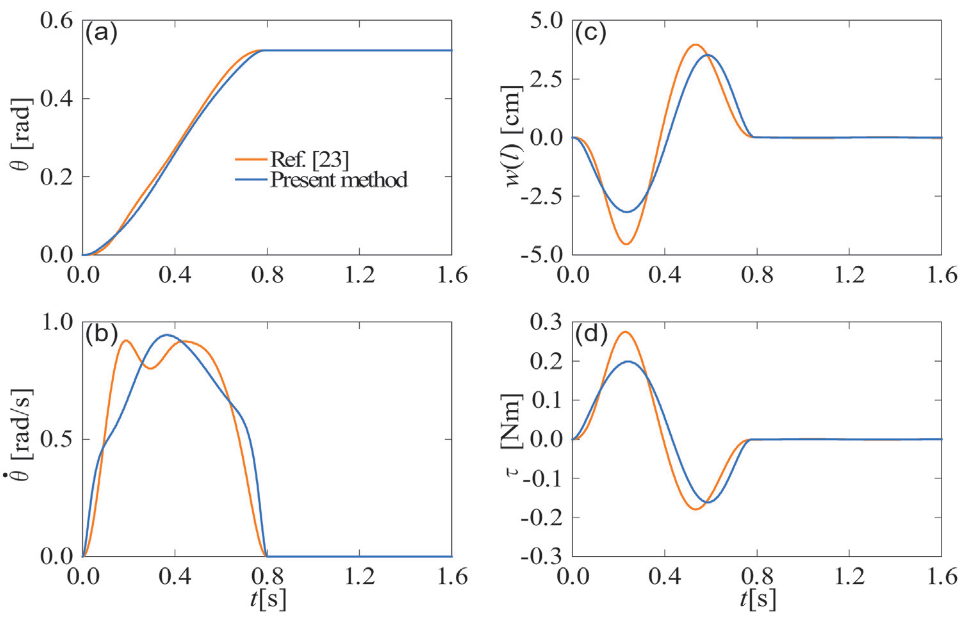

Fig. 3. Comparison of the simulation results obtained by the present method and those obtained by a previous study ($\theta_E = \pi/6$ rad, $T_E = 0.8$ s): (a) joint angle, (b) angular velocity, (c) tip displacement, and (d) motor torque.

Table 3
Comparison of the operating energy F_2 [J] between the previous study in reference 23 and the present method.

θ_E [rad]	T_E [s]	Ref. [23]	Present
$\pi/6$	0.8	6.30×10^{-2}	5.15×10^{-2}
$\pi/2$	1.0	4.21×10^{-1}	2.96×10^{-1}
$\pi/2$	1.1	3.52×10^{-1}	2.23×10^{-1}

3.2. Robotic arm mounted on a flexible link

In this subsection, we deal with a PTP motion of a robotic arm mounted on a flexible link, for which the schematic diagram is presented in Fig. 4. The flexible link is clamped at one end. In the experimental setup [24], we employed an elastic parallel beam, which was made of a brass beam of length 550 mm, width 50 mm, and thickness 1.6 mm, as the flexible link. The center of gravity $\bar{l}$ and mass M of the rigid arm were 105 mm and 450 g, respectively. The joint angle θ of the rigid arm was actuated by an AC servomotor, whose mass m was 635 g. The equations of motion in terms of the flexible link and rigid arm can be written, respectively, as follows:

$$(1 + \alpha_1 \cos\theta)W + 2\zeta\omega\dot{W} + \omega^2 W + (\alpha_2 + \alpha_3 \cos\theta)\theta + \left(\alpha_4 \dot{W}\dot{\theta} - \alpha_3 \dot{\theta}^2\right)\sin\theta = 0, \tag{13}$$

$$\beta_1 \theta + c\dot{\theta} + (\beta_2 + \beta_3 \cos\theta)W = \tau. \tag{14}$$

Here, W is the amplitude of the first vibrational mode of the flexible link and τ is the torque applied at the joint of the rigid arm. The values of the coefficients in Eqs. (13) and (14) are shown below [24]:

$$\left.\begin{array}{l} \alpha_1 = -1.055 \times 10^{-1}[-], \alpha_2 = -9.949 \times 10^{-3}[\mathrm{m}], \alpha_3 = 5.256 \times 10^{-2}[\mathrm{m}], \alpha_4 = 7.634 \times 10^{-2}[-] \\ \zeta = 1.500 \times 10^{-3}[-], \beta_1 = 5.366 \times 10^{-3}[\mathrm{kgm}^2], \beta_2 = -4.944 \times 10^{-3}[\mathrm{kgm}], \beta_3 = 2.399 \times 10^{-2}[\mathrm{kgm}] \\ \omega = 7.320[\mathrm{rad/s}], c = 1.965 \times 10^{-2}[\mathrm{Nms}] \end{array}\right\}. \tag{15}$$

In this subsection, we also attempt to simultaneously minimize the residual vibration of the flexible link and the operating energy of the rigid link when the joint angle θ rotates from the initial angle θ_S to target angle θ_E in travelling time T_E.

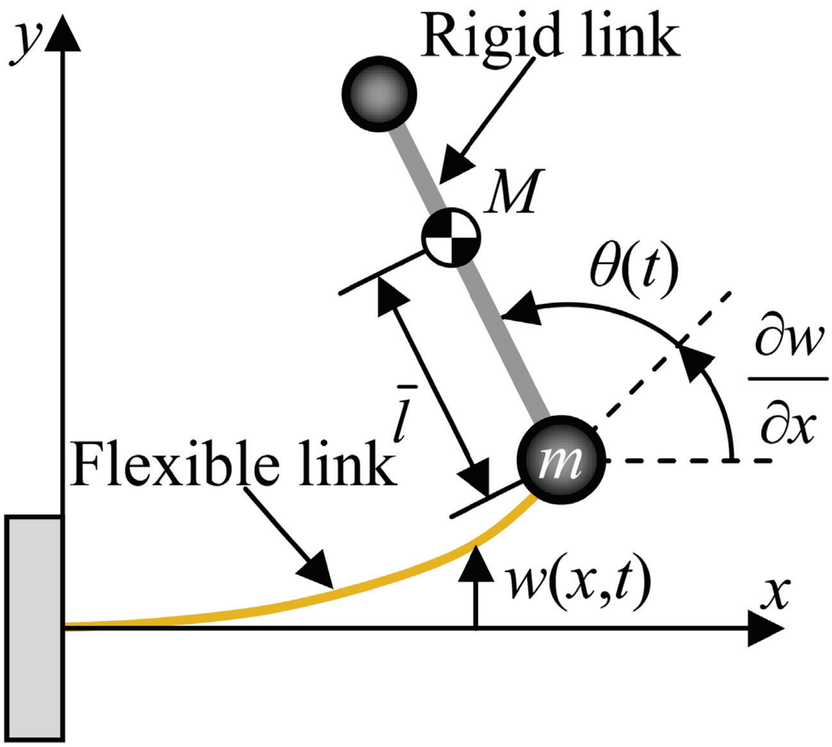

Fig. 4. Schematic of a robotic arm mounted on a flexible link.

Table 4
Optimized parameters under the driving condition ($\theta_S = 0$, $\theta_E = \pi/2$ rad, and $T_E = 0.8$ s).

N	a_1	a_2	a_3	a_4	a_5	a_6
2	-1.023×10^{-1}	-4.365×10^{-1}	–	–	–	–
4	-9.583×10^{-2}	-3.350×10^{-1}	2.090×10^{-1}	-2.854×10^{-1}	–	–
6	-9.346×10^{-2}	-3.488×10^{-1}	1.989×10^{-1}	-1.515×10^{-1}	-2.993×10^{-1}	-2.377×10^{-1}

Thus, we define the following two objective functions:

$$F_1 = \max_{t \in S} [|w(t,l)|], (S : T_E \le t \le T_E + 1\text{s}), F_2 = \int_0^{|\theta_E - \theta_S|} |\tau| d\theta, \tag{16}$$

whose meanings are the same as for Eq. (11). Although the algorithm for the optimal trajectory, which was generated from the simultaneous minimization of the two objective functions in Eq. (16), is tantamount to that of the previous subsection, here we utilized NSGA-II [27] as the multi-objective optimization method.

According to the previous study in reference [24], the number of populations, total number of generations, crossover rate, and mutation rate in NSGA-II are set to 200, 500, 0.8, and 0.01, respectively, for the numerical simulations presented below. The search space of the optimized parameters is defined as follows:

$$a_n \in [-0.5, 0.5], \quad (n = 1, 2, \cdots, N). \tag{17}$$

As in the previous subsection, we examined the effect of the number of terms N in Eq. (6) on the vibration control performance shown in Fig. 5 where the driving condition is set as $\theta_S = 0$, $\theta_E = \pi/2$ rad, and $T_E = 0.8$ s. Table 4 lists the values of the optimized coefficients. It can be observed in Fig. 5(c) that the proposed method cancels the residual vibration for $N \ge 2$ and there is no significant difference in the maximum amplitude during the PTP motion even when the number of terms increases. Here, it should be emphasized that tuning only two coefficients in Eq. (6) by a metaheuristic method can yield the optimal trajectory that suppresses the residual vibration for a complex nonlinear system (see Eqs. (13) and (14)). Consequently, we can say that the proposed method is highly useful as an open-loop vibration control technique. Conversely, as shown in Fig. 5(d), the motor torques obtained from $N = 4$ and 6 rapidly increase immediately after starting. From this, we may infer fact that the operating energy increases with an increase in the number of terms. However, as presented in Table 5, the operating energy decreases with an increasing number of terms. We also confirm from numerical simulations that the energy savings cannot be improved further even when the number of terms is larger than 6. Therefore, we adopt $N = 6$ in the following numerical simulations.

Fig. 6 shows a comparison between the present method (blue line) and previous study (orange line) [24], which utilized radial basis function networks (RBFNs) for an ANN, under the driving conditions ($\theta_S = 0$, $\theta_E = \pi/2$ rad, and $T_E = 0.8$ s). The results obtained by the previous study are similar to those obtained by the present method for $N = 2$. There is no significant

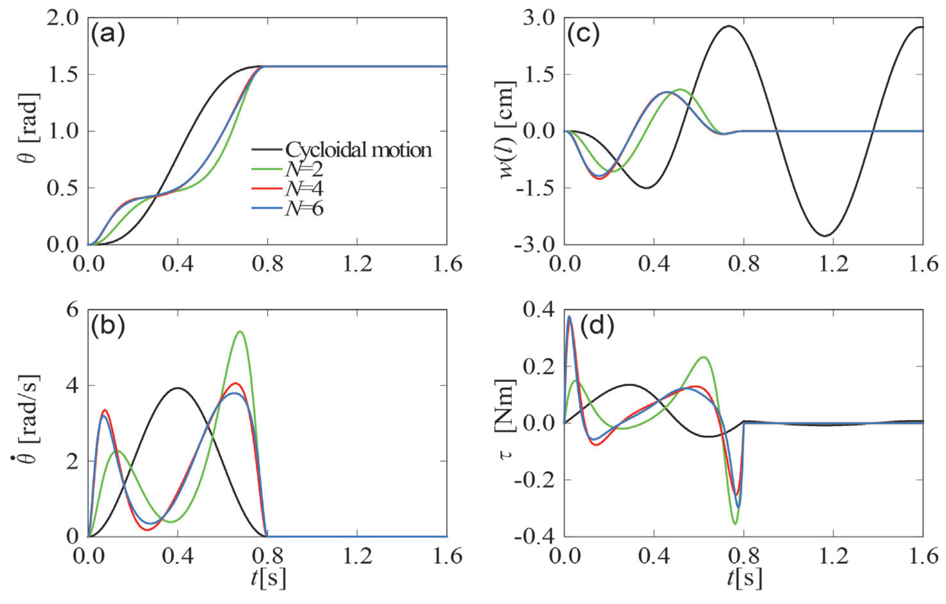

Fig. 5. Effect of the number of terms of the polynomial function on the optimal trajectory ($T_E = 0.8$ s, $\theta_S = 0$, and $\theta_E = \pi/2$ rad): (a) joint angle, (b) angular velocity, (c) tip displacement, and (d) motor torque.

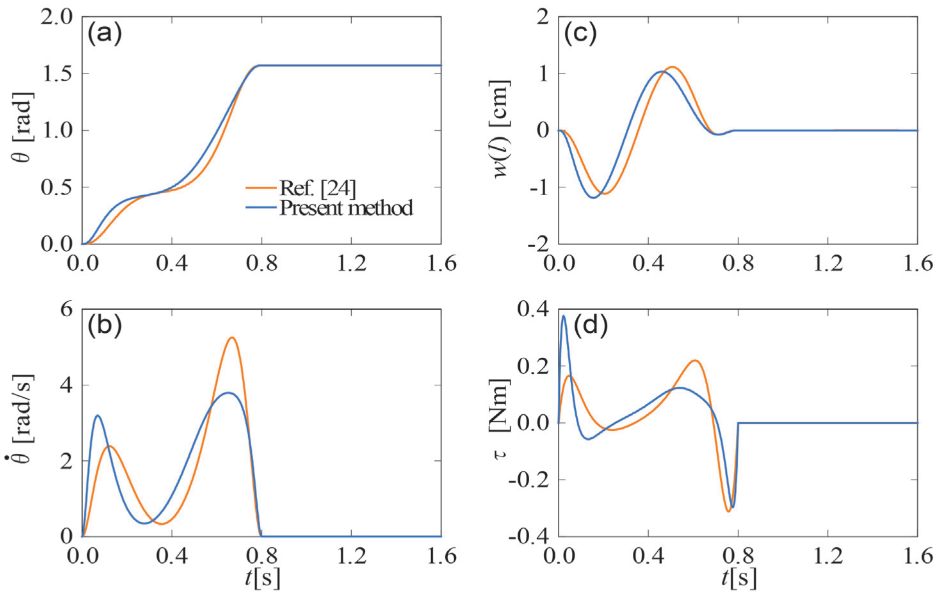

Fig. 6. Comparison of the simulation results obtained by the present method and those obtained by a previous study ($T_E = 0.8$ s, $\theta_S = 0$, and $\theta_E = \pi/2$ rad): (a) joint angle, (b) angular velocity, (c) tip displacement, and (d) motor torque.

Table 5
Effect of the number of terms N on the operating energy F_2 [J] under the driving condition ($\theta_S = 0$, $\theta_E = \pi/2$ rad, and $T_E = 0.8$ s).

$N = 2$	$N = 4$	$N = 6$
2.09×10^{-1}	1.65×10^{-1}	1.49×10^{-1}

Table 6
Comparison of the operating energy F_2 [J] between a previous study in reference 24 and the present method.

θ_S [rad]	θ_E [rad]	T_E [s]	Ref. [24]	Present
0	$\pi/2$	0.8	2.00×10^{-1}	1.49×10^{-1}
$-\pi/2$	$\pi/4$	1.0	1.55×10^{-1}	1.43×10^{-1}
$-\pi/2$	$\pi/2$	1.2	2.22×10^{-1}	2.00×10^{-1}

difference in the vibration control performance of the two approaches. However, the number of tuning parameters (i.e., the parameters of the RBFNs) was 16 in the previous study. Therefore, the proposed method dramatically reduces the number of tuning parameters required to eliminate the residual vibrations. According to the previous study, we consider three driving conditions ($\theta_S = 0$, $\theta_E = \pi/2$ rad, and $T_E = 0.8$ s), ($\theta_S = -\pi/2$, $\theta_E = \pi/4$ rad, and $T_E = 1.0$ s), and ($\theta_S = -\pi/2$, $\theta_E = \pi/2$ rad, and $T_E = 1.2$ s), and then compare the operating energies obtained by the two approaches. Table 6 presents a comparison of the operating energy and indicates that the values obtained by the present method are smaller than those obtained for the previous method for all driving conditions. This is the same as for the single-link flexible manipulator mentioned in the previous subsection. Finally, we can conclude that the optimal trajectory generation proposed here for a PTP motion of a flexible manipulator system achieves further energy saving with zero residual vibrations.

4. Conclusions

This paper presented an investigation of an open-loop control technique for conserving the operating energy of a flexible manipulator system with PTP motion, in which the residual vibration was also suppressed. In the proposed method, the trajectory of the PTP motion task was expressed by a combination of cycloidal and polynomial functions. Since the trajectory profile depends on the coefficients of the polynomial function, the coefficients were tuned using a metaheuristic algorithm so as to minimize the residual vibration and operating energy simultaneously. To evaluate the proposed method, we performed numerical simulations in which a single-link flexible manipulator and a robotic arm mounted on a flexible link were simulated. We confirmed that residual vibration was eliminated by tuning only two coefficients of the polynomial function. Additionally, we compared our results to those of previous studies, thereby demonstrating that the proposed method is superior for energy savings in PTP motion tasks. Therefore, the optimal trajectory planning method developed here has proved to be the more efficient approach for energy saving via residual vibration suppression. An important feature of the present method is that an optimal smooth trajectory caused both residual vibration suppression and energy conservation; the trajectory was generated through a cycloidal function whose input is shaped by a polynomial function in response to a controlled object. The experiments have not been performed at present. However, from the simulation results, it was clear that the proposed method was effective and useful for a PTP motion of a flexible manipulator system. In future, we will perform some experiments to consolidate the validity of the proposed method.

Acknowledgment

This work was partially supported by JSPS KAKENHI Grant Number 26420188.

References

[1] M. Benosman, L.G. Vey, Control of flexible manipulators: a survey, Robotica 22 (5) (2004) 535–545, doi:http://dx.doi.org/10.1017/s0263574703005642.
[2] S.K. Dwivedy, P. Eberhard, Dynamic analysis of flexible manipulators, a literature review, Mech. Mach. Theory 41 (7) (2006) 749–777, doi:http://dx.doi.org/10.1016/j.mechmachtheory.2006.01.014.
[3] H.N. Rahimi, M. Nazemizadeh, Dynamic analysis and intelligent control techniques for flexible manipulators: a review, Adv. Rob. 28 (2) (2014) 63–76, doi:http://dx.doi.org/10.1080/01691864.2013.839079.
[4] K.J. Park, Y.S. Park, Fourier-based optimal design of a flexible manipulator path to reduce residual vibration of the endpoint, Robotica 11 (3) (1993) 263–272, doi:http://dx.doi.org/10.1017/S0263574700016131.
[5] L. Meirovitch, Y. Chen, Trajectory and control optimization for flexible space robots, J. Guid. Contr. Dyn. 18 (3) (1995) 493–502, doi:http://dx.doi.org/10.2514/3.21414.
[6] B. Pond, I. Sharf, Experimental evaluation of flexible manipulator trajectory optimization, J. Guid. Contr. Dyn. 24 (4) (2001) 834–843, doi:http://dx.doi.org/10.2514/2.4785.
[7] K.J. Park, Path design of redundant flexible robot manipulators to reduce residual vibration in the presence of obstacles, Robotica 21 (3) (2003) 335–340, doi:http://dx.doi.org/10.1017/S0263574703005010.
[8] B. Pond, J.V. Vliet, I. Sharf, Prediction tools for active damping and motion planning of flexible manipulators, J. Guid. Contr. Dyn. 26 (2) (2003) 267–272, doi:http://dx.doi.org/10.2514/2.5068.
[9] M. Benosman, G.L. Vey, L. Lanari, A.D. Luca, Rest-to-rest motion for planar multi-link flexible manipulator through backward recursion, J. Dyn. Syst. Meas. Contr. 126 (1) (2004) 115–123, doi:http://dx.doi.org/10.1115/1.1649976.
[10] K.J. Park, Flexible robot manipulator path design to reduce the endpoint residual vibration under torque constraints, J. Sound Vib. 275 (3/5) (2004) 1051–1068, doi:http://dx.doi.org/10.1016/j.jsv.2003.07.001.
[11] H. Kojima, T. Hiruma, Evolutionary learning acquisition of optimal joint angle trajectories of flexible robot arm, J. Robot. Mechatron. 18 (1) (2006) 103–110, doi:http://dx.doi.org/10.20965/jrm.2006.p0103.
[12] F. Ramos, V. Feliu, I. Payo, Design of trajectories with physical constraints for very lightweight single link flexible arms, J. Vib. Contr. 14 (8) (2008) 1091–1110, doi:http://dx.doi.org/10.1177/1077546307080037.
[13] A. Abe, Trajectory planning for residual vibration suppression of a two-link rigid-flexible manipulator considering large deformation, Mech. Mach. Theory 44 (9) (2009) 1627–1639, doi:http://dx.doi.org/10.1016/j.mechmachtheory.2009.01.009.
[14] M.H. Korayem, A. Nikoobin, V. Azimirad, Trajectory optimization of flexible link manipulators in point-to-point motion, Robotica 27 (6) (2009) 825–840, doi:http://dx.doi.org/10.1017/S0263574708005183.
[15] Y. Choi, J. Cheong, H. Moon, A trajectory planning method for output tracking of linear flexible systems using exact equilibrium manifolds, IEEE/ASME Trans. Mechatron. 15 (5) (2010) 819–826, doi:http://dx.doi.org/10.1109/TMECH.2009.2034261.
[16] A. Abe, Trajectory planning for flexible Cartesian robot manipulator by using artificial neural network: numerical simulation and experimental verification, Robotica 29 (5) (2011) 797–804, doi:http://dx.doi.org/10.1017/s0263574710000767.
[17] L. Yihuan, L. Daokui, T. Guojin, Motion planning for vibration reducing of free-floating redundant manipulators based on hybrid optimization approach, Chin. J. Aeronaut. 24 (4) (2011) 533–540, doi:http://dx.doi.org/10.1016/S1000-9361(11)60062-9).
[18] M.H. Korayem, H.N. Rahimi, A. Nikoobin, Mathematical modeling and trajectory planning of mobile manipulators with flexible links and joints, Appl. Math. Model. 36 (7) (2012) 3229–3244, doi:http://dx.doi.org/10.1016/j.apm.2011.10.002.
[19] P. Boscariol, A. Gasparetto, Model-based trajectory planning for flexible-link mechanisms with bounded jerk, Robot. Comput. Integr. Manuf. 29 (4) (2013) 90–99, doi:http://dx.doi.org/10.1016/j.rcim.2012.11.003.
[20] E.J. Solteiro Pires, P.B. de Moura Oliveira, J.A. Tenreiro Machado, Manipulator trajectory planning using a MOEA, Appl. Soft Comput. 7 (3) (2007) 659–667, doi:http://dx.doi.org/10.1016/j.asoc.2005.06.009.
[21] R. Saravanan, S. Ramabalan, Evolutionary minimum cost trajectory planning for industrial robots, J. Intell. Robot. Syst. 52 (1) (2008) 45–77, doi:http://dx.doi.org/10.1007/s10846-008-9202-0.
[22] A. Gasparetto, P. Boscariol, A. Lanzutti, R. Vidoni, Trajectory planning in robotics, Math. Comput. Sci. 6 (3) (2012) 269–279, doi:http://dx.doi.org/10.1007/s11786-012-0123-8.
[23] A. Abe, K. Kimuro, Minimum energy trajectory planning for vibration control of a flexible manipulator using a multi-objective optimization approach, Int. J. Mechatron. Autom. 2 (4) (2012) 286–294, doi:http://dx.doi.org/10.1504/IJMA.2012.050499.
[24] A. Abe, Minimum energy trajectory planning method for robot manipulator mounted on flexible base, Proceedings of the 9th Asian Control Conference, Istanbul, Turkey, 2013, pp. 1–7, doi:http://dx.doi.org/10.1109/ASCC.2013.6606088.
[25] A. Abe, K. Hashimoto, A novel feedforward control technique for a flexible dual manipulator, Robot. Comput. Integr. Manuf. 35 (2015) 169–177, doi:http://dx.doi.org/10.1016/j.rcim.2015.03.008.
[26] K.E. Parsopoulos, D.E. Tasoulis, M.N. Vrahatis, Multi-objective optimization using parallel vector evaluated particle swarm optimization, Innsbruck, Austria, Proceedings of the IASTED International Conference on Artificial Intelligence and Applications, 22004, pp. 823–828.
[27] K. Deb, A. Pratap, S. Agarwal, T. Meyarivan, A fast and elitist multiobjective genetic algorithm: NSGA-II, IEEE Trans. Evolut Comput. 6 (2) (2002) 182–197, doi:http://dx.doi.org/10.1109/4235.99601.